Separation and Purification Technology 66 (2009) 90–97

Contents lists available at ScienceDirect

Separation and Purification Technology

journal homepage: www.elsevier.com/locate/seppur

Membrane characterisation by SEM, TEM and ESEM: The implications of dry and wetted microstructure on mass transfer through integrally skinned polyimide nanofiltration membranes

Darrell A. Patterson[a,*], Alice Havill[a], Sarah Costello[a], Yoong Hsiang See-Toh[b], Andrew G. Livingston[b], Adrian Turner[c]

[a] Department of Chemical and Materials Engineering, Faculty of Engineering, The University of Auckland, Private Bag 92019, Auckland, New Zealand
[b] Department of Chemical Engineering and Chemical Technology, Faculty of Engineering, Imperial College London, Prince Consort Road, London, SW7 2BY, United Kingdom
[c] School of Biological Sciences, Faculty of Science, The University of Auckland, Private Bag 92019, Auckland, New Zealand

ARTICLE INFO

Article history:
Received 1 February 2008
Received in revised form 17 November 2008
Accepted 25 November 2008

Keywords:
Polyimide
Pore flow
Solution diffusion
Transmission electron microscopy
Environmental scanning electron microscopy
Organic solvent nanofiltration

ABSTRACT

Due to their excellent resistance to a range of solvents, integrally skinned polyimide membranes have been used to achieve selective separations in a range of solvent-based industrial and lab-scale chemical operations. These include: homogeneous catalyst recycle, petrochemical dewaxing, solvent exchange and chiral resolutions. However, despite the widening scope of use of these membranes, there is still little understanding of how the microstructure defines their separation performance. As a first step towards determining this, integrally skinned nanofiltration membranes were fabricated by phase inversion using Lenzing P84 polyimide. The microstructures of these membranes, dry and wetted in solvent, were investigated by SEM, TEM and ESEM (where appropriate).

SEM and TEM imaging of dry membranes revealed that this type of polyimide membrane has three microstructurally distinct polyimide layers, not the two indicated in prior literature. Furthermore, TEM images reveal nano-sized pore-like features in the polyimide structure, which indicate that the transport mechanism is probably neither only solution-diffusion nor only pore flow. ESEM imaging showed that when saturated in ethanol at the working pressure of the ESEM (5.50 Torr), the microstructure of the membranes changes; it is wispy and thus quite different to the more solid polymer nodules and interconnected polymer network observed in the dry membranes. Thus, transport and separation mechanisms based on the structure of the dry membranes may not be accurate. Overall, these results indicate that the current theory used to describe polyimide membrane mass transfer and separation performance (where it is based on dry membrane microstructures), most likely needs to be rethought.

1. Introduction

Lenzing P84 (BTDA-TDI/MDI, co-polyimide of 3,3′,4,4′-benzophenone tetracarboxylic dianhydride and 80% methylphenylenediamine + 20% methylene diamine; Fig. 1) is a co-polymer which has recently been identified as a robust material for the preparation of membranes for ultrafiltration, nanofiltration, gas separation and pervaporation [1] due to its excellent solvent resistance. A number of recent studies have looked at the formation of these P84 co-polyimide membranes [1–11].

This study concerns only Lenzing P84 nanofiltration membranes. Such nanofiltration membranes have been found to be effective for many applications, in particular for non-aqueous filtrations (organic solvent nanofiltrations) such as separating of solvents from lube oil and the separation of aromatics [2–4], recycling homogeneous catalysts and bases [12–15], separating chiral diastereomers [16] and green organic synthesis [17]. Despite the widening scope of use of these membranes, there is still little understanding of how the microstructure defines their separation performance in solvent-based operations. In particular, the following questions are yet to be answered: (1) What is the transport mechanism through these membranes in organic solvent nanofiltrations (i.e. how do we reliably predict the separation that these membranes give)? (2) What is their microstructure? (3) How do different solvents affect their microstructure and how does this impact on the separation performance?

Despite not having understood the microstructure of the membranes, the transport mechanism through these membranes has been attempted to be modelled, typically using models that are related to the dry membrane microstructure. The two most commonly used are:

* Corresponding author. Tel.: +64 9 373 7599; fax: +64 9 373 7463.
E-mail address: darrell.patterson@auckland.ac.nz (D.A. Patterson).

1383-5866/$ – see front matter © 2008 Elsevier B.V. All rights reserved.
doi:10.1016/j.seppur.2008.11.022

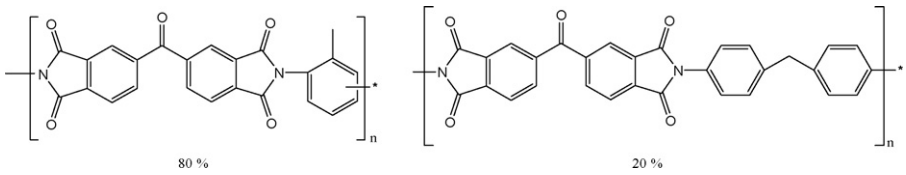

Fig. 1. Chemical structure of P84 co-polyimide.

1. The solution-diffusion model [18–20], which is typically used to describe transport through pore-less membranes, like those used in reverse osmosis. The solution-diffusion model assumes that the permeating species dissolves in the membrane material and diffuses through the membrane down a concentration gradient. A separation is achieved between different solutes due to differences in the amount that dissolves in the membrane and the rate at which it diffuses through the membrane [18–20].
2. The pore-flow model [18–20], which is used to describe the permeation through porous membranes (ultrafiltration, microfiltration). It describes the separation based on pressure-driven convective flow through tiny pores. Selectivity results from exclusion, based on incompatibility of molecule parameters such size, shape and charge, with the pores in the membrane.

Nanofiltration membranes, including these Lenzing P84 membranes, are used for molecular separations. Such separations occur in the transition between ultrafiltration and reverse osmosis membrane operations [19,20], separating molecules with molecular weights of 200–1000 g mol^{-1}. Therefore without resolving the microstructure of these membranes, it is uncertain which of the above mechanisms (or indeed a combination of both) governs mass transport through nanofiltration membranes.

Consequently, attempts have been made to resolve the microstructure of Lenzing P84 nanofiltration membranes. It has been reported [4] that these integrally skinned co-polyimide membranes have a three layer structure (Fig. 2), with polyimide split into a dense separation layer and a porous support layer that gives little resistance to mass transfer compared to the skin layer. A polyester non-woven support layer typically adds strength to this matrix. However, this type of microstructure does not correlate with some filtration results obtained with Lenzing P84 membranes. It has been assumed in the past that this sort of dense skin layer implies that separation is best described by solution-diffusion [20]. However, Patterson et al. [15], for example, concluded that for the organic solvent nanofiltration of trialkylamine bases, the main transport mechanism was pore flow with solution diffusion becoming significant if the concentration at the membrane caused by concentration polarisation and/or fouling becomes sufficient. Pore-flow cannot be excluded as a mechanism, since in the prior literature there has been no evidence establishing the presence or absence of pores or pore-like features (which in this context could

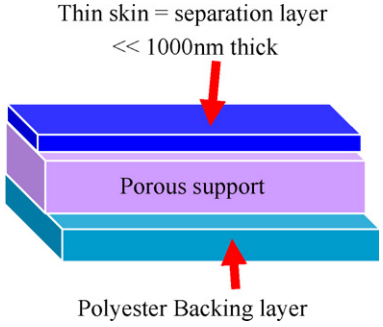

Fig. 2. Microstructure of Lenzing P84 nanofiltration membrane based on White [4].

be fixed nano-scale voids between polymer chains and/or clusters of polymer, aligned into channels, or a fluctuating free volume that could act like pores). Consequently, a more detailed analysis of these membranes could reveal very different microstructure to what has been previously established. Moreover, Vankelecom et al. [21] have demonstrated that the transport mechanism through MPF-50 and PDMS membranes depends on the physico-chemical nature of these membranes. Consequently, the transport mechanism can change depending on the filtration conditions, as seen in the results by Patterson et al. [15]. Very thin porous top layers, very viscous solvents, strongly swelling solvents, low top layer porosities and high pressures, all make the porous support dominate the transport mechanism, giving convective flow [21]. This all indicates that a more detailed investigation of this nature is required for Lenzing P84 membranes, investigating the physio-chemical properties of the membrane in order to clarify the relationship between microstructure and transport mechanism.

In order to do this, the microstructure of the membranes must be imaged and characterised. This is typically done using dry membranes. However, during an organic solvent nanofiltration, the structure of the membrane changes when in contact with the solvent to be used, especially due to swelling [8]. Therefore, although imaging a membrane outside of a solvent (i.e. dry) may give an indication of the initial microstructure prior to filtration, in order to understand how the microstructure affects the transport mechanism and thus membrane separation performance when it is being used, the membrane must be imaged when in solvent (i.e. wetted).

Consequently, as a first step towards addressing these issues, integrally skinned nanofiltration membranes were fabricated by phase inversion using Lenzing P84 polyimide. The microstructure of these membranes were characterised using a scanning electron microscope (SEM) and a transmission electron microscope (TEM) for dry membranes and an environmental scanning electron microscope (ESEM) for ethanol wetted membranes. The implications of these microstructures to the aforementioned filtration results and the transport mechanism through these membranes were then considered.

2. Materials and methods

2.1. Polyimide membrane fabrication

Membranes were fabricated from P84 co-polyimide (CAS# 58698-66-1, HP polymer GmbH) which was used as received. The main membrane characterised (hereafter referred to as M1) was fabricated with 22 wt% P84 and any additives were dissolved in dimethylformamide (21 wt%) and 1,4-dioxane (57 wt%). This was stirred continuously at 50 °C overnight to obtain a homogeneous dope solution. Following this, the polymer solution was allowed to stand at room temperature for 24 h to remove air bubbles. 200 mm thick polyimide films were then cast on a non-woven polyester backing material (Holytex 3329) using an adjustable doctor blade casting knife on an automatic film applicator (Braive Instruments). The solvent was allowed to evaporate from the surface of the film for approximately 10 s before immersion into a water bath at room temperature overnight. The membranes were subsequently immersed in solvent exchange baths of isopropanol

Table 1
The composition of dope solution, the evaporation time and the heat treatment temperature used to vary membrane formation parameters for Lenzing P84 membranes M2–M7, fabricated using NMP, DMSO and Acetone as dope solution solvents and characterised by SEM and ESEM.

Membrane	Dope solution composition (wt%)				Heat treatment temperature
	P84	NMP	DMSO	Acetone	
M2	25	56.25	18.75	–	–
M3	25	75	–	–	–
M4	25	65	–	10	–
M5	25	75	–	–	100 °C
M6	25	75	–	–	150 °C
M7	25	75	–	–	200 °C

and then toluene to remove any residual DMF and water. Finally, the membranes were immersed in a mineral oil bath. This oil mixture soaked into the membrane, allowing them to be handled outside of a solvent bath. Without this conditioning oil, the membrane cracked when allowed to dry (for further details on these membranes see: See-Toh et al. [11]). The molecular weight cut-off (MWCO) in toluene for these membranes was 260 g mol^{-1} [11]. For membrane M1, all chemicals and solvents were obtained from Sigma–Aldrich, UK.

Further membranes were fabricated (Table 1: membranes M2–M7) using Lenzing P84 co-polyimide at 18–25 wt% with n-methyl-2-pyrrolidone (NMP), dimethyl sulfoxide (DMSO) and acetone as solvents following the same procedure as above, except the membranes were cast on glass only, and not on a polyester backing layer. Furthermore, membranes M5–M7 were heat treated at 100, 150 and 200 °C after the final solvent exchange step with the mineral oil (Sigma–Aldrich, Cat No.: 330779), in order to increase the skin layer density (as has been shown in previous work [11]). Membranes M2–M7 were then used to confirm the generality of the structural features that were determined for membrane M1 by SEM and ESEM.

Membrane M1 was fabricated by the team at Imperial College, London then prepared and imaged by the team at the University of Auckland. Membranes M2–M7 were fabricated, prepared and imaged by the team at the University of Auckland.

2.2. Analytical techniques

2.2.1. Scanning electron microscopy (SEM)

Membranes were cut into samples of size 5 mm × 5 mm either with a knife or using liquid nitrogen, then placed in hexane overnight (to remove the conditioning oil). After, the samples were dried for 15 min and then broken 90° to the membrane surface so that the cross-section was exposed. Each sample was mounted on a support using carbon tape to secure the sample and platinum coated by a sputter coater (Polaron SC 7640) at 1.1 kV for 180 s. Once coated, the membrane samples were inserted into the Field Emission SEM (Philips XL30S Field Emission Gun), and imaged using an acceleration voltage of 3–5 kV. Imaging focussed on the structure of the membrane cross-section and top layer surface.

2.2.2. Transmission electron microscopy (TEM)

Membranes were placed in hexane overnight (to remove the conditioning oil), after which they were dried for 15 min. Approximately 1 mm × 3 mm sections were cut from the filter with a razor blade and placed in flat embedding moulds. They were covered with EM bed-812 epoxy resin (Electron Microscopy Sciences, Fort Washington, PA, USA) which was polymerised at 60 °C for 48 h. The resin blocks were trimmed to expose the filter in cross section, and were marked to indicate the coated face of the filter. One block was selected for ultramicrotomy on an LKB Ultrotome Nova ultramicrotome, using a 45° diamond knife (Diatome, Switzerland). Cross-sections of approximately 60 nm thickness were collected onto 400-mesh copper TEM grids. The sections were stained for 20 min with 2% (w/v) aqueous uranyl acetate, washed six times with distilled water and air-dried. Sections were viewed in a CM12 TEM (Philips, Eindhoven, The Netherlands) operating at an accelerating voltage of 120 kV, and images were recorded using a 1024 × 1024 pixel Bioscan digital camera (Gatan, Pleasanton, CA, USA).

2.2.3. Environmental scanning electron microscopy (ESEM)

Membrane M1 was reduced into samples of size of 50 mm × 50 mm using either a knife or breaking in liquid nitrogen. The backing layer was not removed so that it could also be imaged. The samples were then soaked in ethanol for an hour. The soaked membranes were removed from solution and further cut into smaller samples of approximately 2 mm × 2 mm. The top layers of the membrane sample were exposed by breaking the sample 90° to the membrane surface in order to reveal the polyimide layers in the cross-section. Note that the more elastic polyester backing layer was not broken. These samples were placed in the vacuum dish of the ESEM (FEI Quanta 200F) and arranged into position using aluminium foil as support. Once secure, the samples inside the vacuum dish were soaked in ethanol using a syringe. The vacuum chamber was then sealed and pressurized and the sample was imaged. The ESEM conditions were: HV, 20.0 kV, pressure 5.50 Torr, spot.

To determine if the microstructures imaged for membrane M1 were the result of wetting with ethanol, membranes M2–M7 (Table 1) were filtered with ethanol in a SEPA ST (Osmonics, USA) cell with an effective membrane area of 13.9 cm^2. The experimental setup was similar to that used in previous work [12,16,22]. Nitrogen gas was applied as the pressure driving force and the filtrations were all conducted at the same stirrer speed. The membranes were left soaking in ethanol after the filtration. For the 'wetted' images, the soaked membranes were removed from solution and cut into sample sizes of 10 mm × 5 mm. The samples were placed in the vacuum dish of the ESEM (FEI Quanta 200F) and arranged into position using aluminium foil and rectangular brass rods as support, then imaged as previously described. For the 'dry' images, the membranes were removed from the ethanol and left to dry in a fume hood for one hour. The membranes were then cut into sample sizes of 10 mm × 5 mm, prepared for imaging as above and imaged by ESEM as previously described.

3. Results and discussion

3.1. SEM and TEM

SEM imaging (Fig. 3) and TEM imaging (Fig. 4) revealed that when dry, this type of polyimide membrane has three distinct polyimide microstructures, not two as previously indicated [4]. This means that these Lenzing P84 phase inversion nanofiltration membranes actually consists of four microstructurally distinct layers (Fig. 5):

1. The top skin layer, which consists of closely packed polymer nodules (Fig. 3b). These nodules are not artefacts of the platinum sputter coating of the membranes and are a feature of the top layer microstructure, since SEM images of titanium dioxide and zinc oxide thin films on glass using the same sputtering technique and instruments do not show these nodules [23,24]. The TEM images represent thin slices through the top layers of the membrane, giving an essentially two-dimensional image of a cross-section through the three-dimensional nodules in the SEM images. The dark regions represent the polyimide and the light

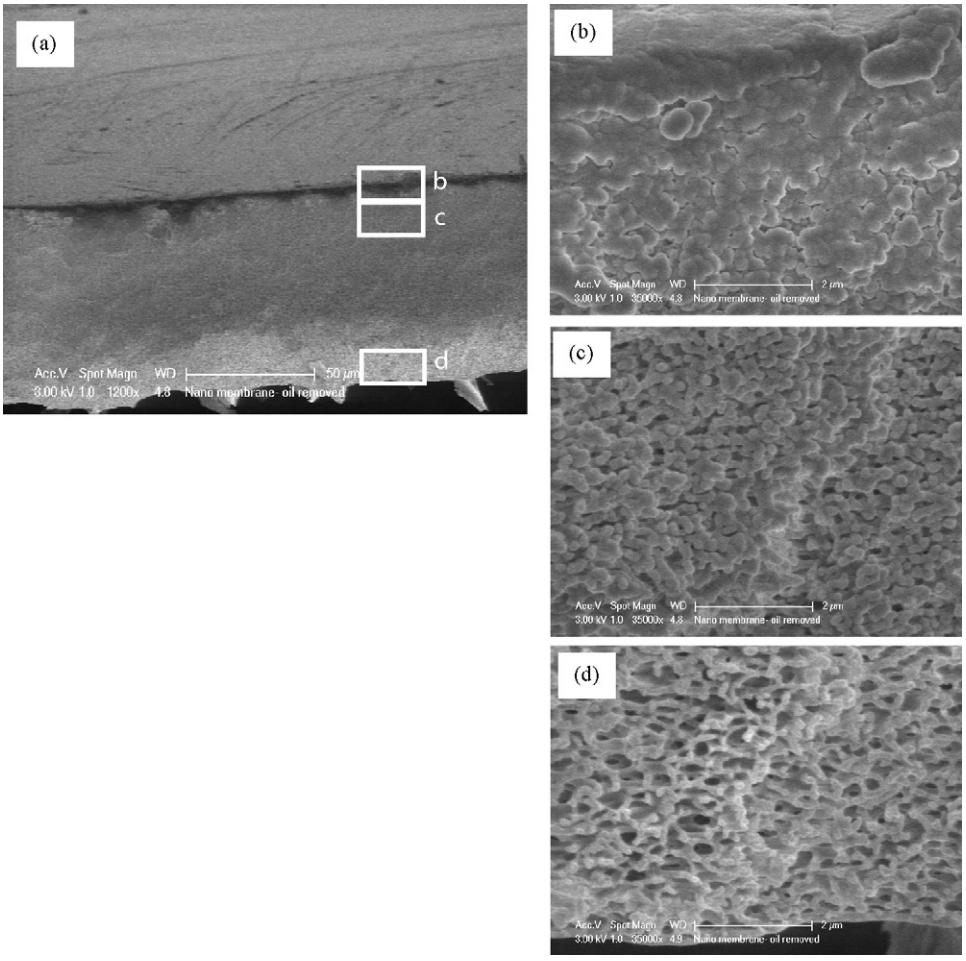

Fig. 3. SEM images of a cross-section of the Lenzing P84 membrane M1, showing: (a) overall microstructure, (b) top layer consisting of closely packed polymer nodules, (c) below the top layer—a microstructure transition region where the nodules slowly become more interconnected further from the membrane, eventually becoming and (d) a uniformly porous support layer consisting of an interconnected polyimide network.

regions represent the EM bed-812 epoxy resin used to hold and preserve the structure for cross-sectioning into thin slices. Therefore, in the TEM images (Fig. 4), the closely packed nodules of the top layer are the more uniformly structured layer near the surface that has polymer aligned perpendicular to the membrane surface, giving a microstructure which resembles crepe paper.

2. A microstructure transition region where the microstructure changes, with the densely packed polymer nodules slowly becoming more interconnected and less densely packed further from the membrane surface. The microstructures in this region can be clearly distinguished in the SEM images (Fig. 3c), however the precise starting point cannot be determined. In the TEM

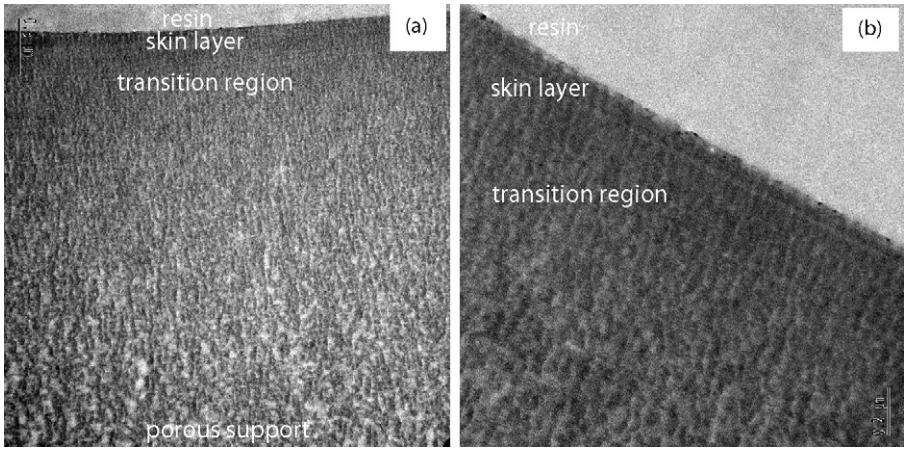

Fig. 4. TEM images of a cross-section of the 'dry' Lenzing P84 membrane M1, showing: (a) the overall microstructure and (b) structure of the top layer and the microstructure transition region. N.B. TEM images are two-dimensional, thus reveal the structure through a thin cross-section of the membrane. The dark regions are the polyimide and the light regions are the EM bed-812 epoxy resin used to fix the structure for cross-sectioning using ultramicrotomy.

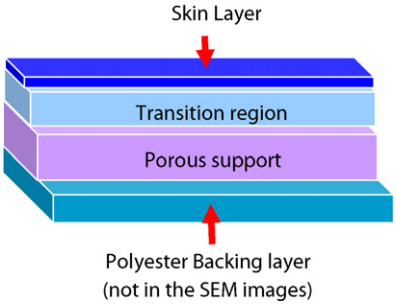

Fig. 5. Schematic of the proposed four microstructurally distinct layer structure for the P84 nanofiltration membranes.

images (Fig. 4), the start of the transition region can be seen to be when the aligned skin layer microstructure becomes disordered and the structure becomes less densely packed.

3. A uniformly porous support layer consisting of an interconnected polyimide network. This interconnected polymer network is illustrated well by SEM (Fig. 3d), and is illustrated in TEM images where the polyimide regions (the dark regions) become evenly spaced and the dark–light pattern of the polyimide and the resin filled free volume becomes uniform (Fig. 4).
4. The non-woven polyester backing sheet the membrane was cast on. This layer was removed for both SEM and TEM imaging, so does not appear in Figs. 3, 4 and 6.

The team at Imperial College have previously observed this four-layered structure in dry membranes using SEM imaging [11]. The TEM images in Fig. 4 also confirm that it is not an artefact of the SEM sample preparation used or the SEM imaging. Furthermore, this four layered structure is also observed in the SEM images of membranes M2–M7 (results not presented). This type of structure has been proposed for other membranes (e.g. Kazama and Sakashita [25]) and has been observed by Qiao et al. [1] previously in P84 pervaporation membranes.

As mentioned previously, prior to this project there is no evidence establishing the presence or absence of pores or pore-like features for this type of polyimide membrane. The SEM images (Fig. 3a and b) are not conclusive on whether or not there are these types of features either. However, the TEM images (Figs. 4b and 6) reveal that in these dry membranes, nano-sized pore-like features run from the surface of membrane, through the skin layer and into the interior of the membrane. The pore-like features are perpendicular to the membrane top surface (which is the interface between the lighter resin at the top of the image, and the darker polyimide membrane cross-section), then become more interconnected and irregular further down from this surface. The tortuosity of the pore-like features therefore increases at the start of the transition region (Fig. 6), indicating that the transition region, and not just the skin layer, should affect the mass transfer resistance and selectivity of the membrane. The size of these pore-like features is representative of the sample preparation conditions of the membrane: acetone swollen and treated with EM bed-812 epoxy resin to fix the structure for cross-sectioning using ultramicrotomy. The large swelling expected in an acetone saturated membrane therefore means that there are large pore-like features at the membrane surface in these TEM images: the cross-sectional length at the surface of these pore-like features is 10–15 nm based on Fig. 6. Note that the size of these pore-like features is not directly related to the aforementioned 260 Da MWCO, which was the result of filtration of this membrane in toluene. In this case the membrane would be less swollen, which hypothetically would give the smaller pore-like features.

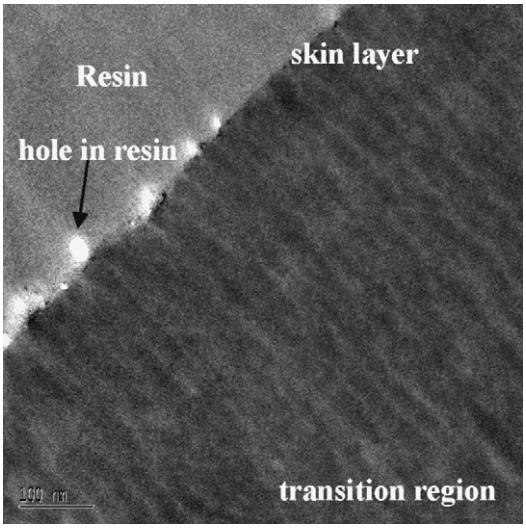

Fig. 6. TEM image of a cross-section of the 'dry' Lenzing P84 membrane M1, showing a close-up of the top skin layer. This shows pore-like features connecting to the top active surface of the membrane. The dark regions are the polyimide and the light regions are the EM bed-812 epoxy resin used to fix the structure for cross-sectioning using ultramicrotomy.

The Imperial team have also suggested that these pore-like features could exist in dry membranes like M1 based on their SEM images [11]. The TEM images here provide definitive confirmation.

The TEM images also provide two important characteristic lengths of these membranes previously unquantifiable by the more commonly used SEM. Firstly, the TEM images provide a definitive way of determining the thickness of the top layer of the membrane. Currently there is no widely accepted definition for the top layer thickness. Based on the morphology observed here, it is proposed that the skin layer thickness be defined as the length perpendicular from the surface of the membrane to the point where these pore-like features become interconnected i.e. the point at which the microstructure begins to transition into the more interconnected network of the porous support, which is therefore where the microstructure transition region begins. Based on Fig. 6, this means that the top layer thickness of membrane M1 is 110–130 nm. Secondly, the TEM images also show where the transition region ends and the porous support begins (as described above). Since the TEM images also show where the microstructure transition region begins (i.e. where the top layer ends), these TEM images also allow the determination of the thickness of the transition region. Therefore the thickness of the transition region is proposed to be the length perpendicular from the surface of the membrane between these two points. Unfortunately, insufficient TEM images were taken to accurately determine the transition region thickness for membrane M1. Consequently, imaging 'dry' membranes by TEM not only reveals microstructural features that are difficult to visualise by SEM (here the pore-like features), but also allows the quantification of two characteristic lengths in the membrane microstructure. Note that these characteristic lengths will only be representative of the sample preparation conditions of the membrane however: here this means acetone swollen and treated with EM bed-812 epoxy resin. Further work is continuing to quantify and/or extrapolate these features to membranes in other solvents.

The presence of nano-sized pore-like features in these membranes reconciles some of the filtration data that does not fit well with the previously proposed microstructure. The membrane structure proposed here correlates well with the results obtained by Patterson et al. [15] who found that in the toluene nanofiltration of trialkylamine bases, the transport mechanism was most likely pore flow. Solution diffusion became significant for large molecules such as the tridodecylamine when the concentration at the membrane

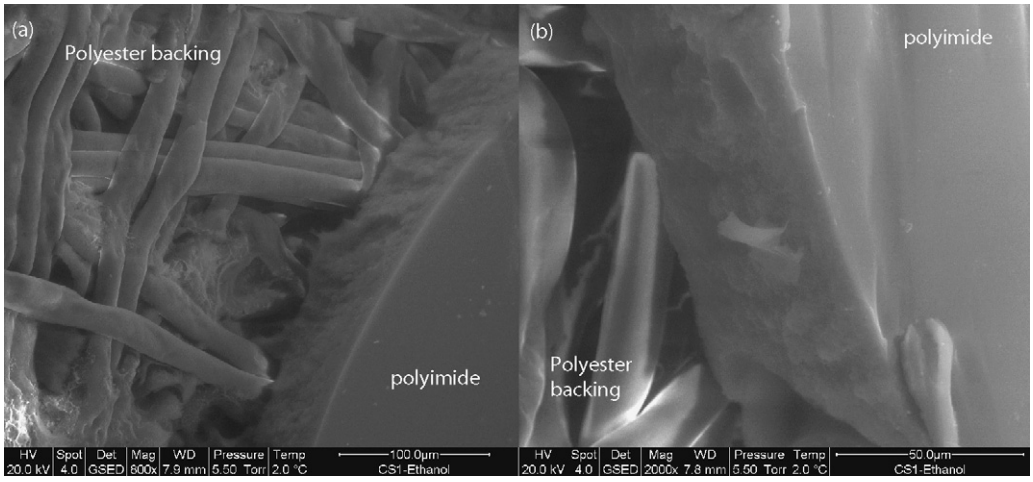

Fig. 7. ESEM images of the polyimide nanofiltration membrane M1 saturated in ethanol: (a) The woven backing layer is shown to the left of the image as the thread-like structure. The polyimide layers are shown as the block section on the right of the image. (b) The polyimide layers—unfortunately the separation between the skin layer and the other layers cannot be resolved at this low magnification.

caused by concentration polarisation and/or fouling became sufficient. This can now be reconciled to the membrane microstructure: the pore-like features are so small that when contacted by tridodecylamine (which is unlikely to pass through these pore-like voids), the membrane is essentially a dense film composite of polyimide and solvent (in the pore-like voids). This composite polyimide-solvent membrane would have different properties than polyimide and solvent alone, including partitioning coefficients. This difference in membrane properties may be overlooked in mathematical modelling of mass transport through these membranes and could partly explain why models of nanofiltration operations using these sorts of membranes often do not correlate well with experimental data.

3.2. ESEM

Membranes are always used whilst in contact with the fluid medium containing the solutes that are to be separated—i.e. for liquid separations like organic solvent nanofiltrations, they are used when 'wet'. However the vast majority of microstructural imaging of membranes used for liquid separations is performed on dry membranes. This is despite the fact that it is known that the structure of the membrane changes when in contact with the solvent to be used for the filtration, especially due to swelling [8]. To understand how the microstructure affects the membrane separation performance when wetted by solvent, the membrane has been imaged using an ESEM with the membrane sample saturated in ethanol at 5.50 Torr (0.733 kPa). Note that since this low pressure must be used, the membrane is not wetted with ethanol to the same degree that it would be were in use (which would typically be at pressures above 101.3 kPa). However, the membrane should still be saturated with more ethanol than the dry membranes imaged by SEM in this work and others. The images therefore give an indication of how the membrane microstructure would differ in an SEM type image in the presence of ethanol (i.e. wetted), compared to how to when imaged by normal SEM.

This ESEM imaging of membrane M1 showed that when saturated in ethanol, the microstructure of the membrane appears different (Fig. 7). Although the magnification of the images in Fig. 7 is low, it can be observed that the polyimide layers in the membrane are 'wispy' and 'fluffy' (somewhat like wet cotton wool), and thus quite different to the three polyimide layers imaged for the dry membranes in Section 3.1, which consist of structures ranging from solid polymer nodules to an interconnected polymer network. It is possible that the difference in microstructures is due to the 1 h pre-saturation in ethanol (not used for the SEM samples), which could have allowed the polyimide to swell and rearrange. This could mean that the microstructure imaged (although differ-

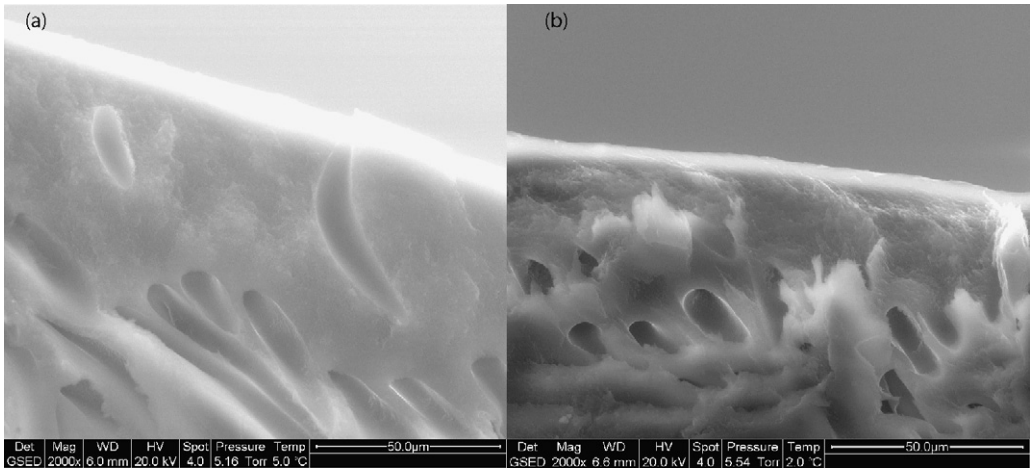

Fig. 8. ESEM images of the top layers of polyimide nanofiltration membrane M2 (25 wt% P84 polyimide, 56.3 wt% NMP, 18.75 wt% DMSO, 10 s Evaporation, post-filtration and ethanol presaturation) at 2000× magnification: (a) dry and (b) saturated in ethanol.

ent) is not representative of the ethanol wetted microstructure. To eliminate this possibility, membranes M2–M7 were subjected to the 1 h ethanol pre-saturation and then were imaged both unsaturated and saturated with ethanol. Getting sufficient resolution to see clear structural details is very challenging when using ESEM, consequently only membrane M2 gave detailed enough images that could be used for comparison (Fig. 8). Never-the-less, Fig. 8 demonstrates that the 'wispy' and 'fluffy' microstructure is present in the ethanol wetted membrane in the ESEM and not in the 'dry' membrane, despite the 1 h pre-saturation of both membrane samples, indicating that the difference in microstructure seen in the ESEM images may be attributed to the ethanol wetting. These results therefore demonstrate that the microstructures observed in dry membranes may change significantly when in solvent. Consequently, any transport and separation mechanisms in the literature based on the microstructures of dry membranes may not accurately reflect the microstructure of wetted membranes and therefore most likely need to be rethought.

The resolution in the current ESEM results have not allowed us to distinguish the changes in the aforementioned three microstructurally distinct polyimide layers when the membrane is in the solvent. Thus, further work is continuing imaging these membranes in ethanol and other solvents, at higher magnification, to elucidate their wetted microstructure in more detail, especially to determine the effect of solvents on the pore-like features observed in the dry membranes.

4. Conclusions

For integrally skinned nanofiltration membranes fabricated by phase inversion using Lenzing P84 polyimide:

- SEM and TEM imaging revealed that this type of polyimide membrane, when dry, has three microstructurally distinct polyimide layers: a nano-porous nodular top layer, a uniformly porous support layer consisting of an interconnected polyimide network and a layer in-between these two where the microstructure transitions from that of the top layer to that of the porous support.
- TEM images revealed that in the dry membranes there are pore-like features (nano-sized voids between polymer chains and/or nodules of polymer that are aligned into channels) perpendicular to the membrane top surface (skin layer), which then become more interconnected further down from this surface. The presence and size of these nano-sized pore-like features indicate that the transport mechanism is probably neither only solution-diffusion nor only pore-flow.
- Based on the TEM images of membrane M1, the thickness of the skin layer of these membranes was proposed to be defined as: the length perpendicular from the surface of the membrane to the point where these pore-like features become interconnected; i.e. the point at which the microstructure begins to transition into the more interconnected network of the porous support. For the main membrane studied (M1), this means the top layer thickness was between 110 and 130 nm.
- A definition of the thickness of the microstructure transition region was also proposed based on the TEM images of membrane M1. The thickness of the transition region is proposed to be defined as being the length perpendicular from the surface of the membrane from where the skin layer ends (as defined above) to where the polyimide regions become evenly spaced and the dark–light pattern of the polyimide and the resin filled free-volume in the TEM image becomes uniform. At this point there is a uniformly porous microstructure, which is characteristic of the porous support.
- ESEM imaging showed that when saturated in ethanol, the microstructure of the polyimide layers are different to the three polyimide layers described for the dry membranes. Thus, transport and separation mechanisms based on the structure of the dry membranes may not be accurate.
- Overall, these results indicate that the current theory used to describe polyimide membrane separation performance, where based on dry membrane microstructures, most likely needs to be rethought.

Acknowledgements

The authors would like to thank Catherine Hobbis and Bryony James at the Research Centre for Surface and Materials Science at the University of Auckland for training and guidance of the SEM and ESEM imaging.

Thank you also to the Royal Society of New Zealand's Bilateral Research Activities Programme of the International Science and Technology (ISAT) Linkages Fund, contract ISATA06-76, for supporting the University of Auckland and Imperial College collaboration.

Thanks also to the Department of Chemical and Materials Engineering at the University of Auckland, for funding the analysis in this project.

References

[1] X. Qiao, T.-S. Chung, K.P. Pramoda, Fabrication and characterisation of BTDA-TDI/MDI (P84) co-polyimide membranes for the pervaporation dehydration of isopropanol, J. Membr. Sci. 264 (2005) 176–189.
[2] L.S. White, I-F Wang, B.S. Minhas, Polyimide membrane for separation of solvents from lube oil, United States Patent 5,264,166, November 23, 1993.
[3] L.S. White, Polyimide membranes for hyperfiltration recovery of aromatic solvents, United States Patent, US 6,180,008 B1, 2001.
[4] L.S. White, Transport properties of a polyimide solvent resistant nanofiltration membrane, J. Membr. Sci. 205 (2002) 191–202.
[5] J.N. Baresema, G.C. Kapantaidakis, N.F.A. van der Vegt, G.H. Koops, M. Wessling, Preparation and characterization of highly selective dense and hollow fiber asymmetric membranes based on BTA-TDI/MDI co-polyimide, J. Membr. Sci. 216 (2003) 195–205.
[6] D. Li, T.-S. Chung, J. Ren, R. Wang, Thickness dependence of macrovoid evolution in wet phase-inversion asymmetric membranes, Ind. Eng. Chem. Res. 43 (6) (2004) 1553–1556.
[7] R. Liu, X. Qiao, T.-S. Chung, The development of high performance P84 co-polyimide hollow fibers for pervaporation dehydration of isopropanol, Chem. Eng. Sci. 60 (2005) 6674–6686.
[8] X. Qiao, T.-S. Chung, Fundamental characteristic of sorption, swelling, and permeation of P84 co-polyimide membranes for pervaporation dehydration of alcohols, Ind. Eng. Chem. Res. 44 (23) (2005) 8938–8943.
[9] J. Ren, Z. Li, F.-S. Wong, Membrane structure control of BTA-TDI/MDI (P84) co-polyimide asymmetric membranes by wet-phase inversion process, J. Membr. Sci. 241 (2004) 305–314.
[10] J. Ren, Z. Li, F.-S. Wong, D. Li, Development of asymmetric BTDA-TDI (P84) co-polyimide hollow fiber membranes for ultrafiltration: the influence of shear rate and approaching ratio on membrane morphology and performance, J. Membr. Sci. 248 (2005) 177–188.
[11] Y.H. See-Toh, F.C. Ferreira, A.G. Livingston, The influence of membrane formation parameters on the functional performance of organic solvent nanofiltration membranes, J. Membr. Sci. 299 (2007) 236–250.
[12] J.T. Scarpello, D. Nair, L.M.F. dos Santos, L.S. White, A.G. Livingston, The separation of homogeneous organometallic catalysts using solvent resistant nanofiltration, J. Membr. Sci. 203 (1–2) (2002) 71–85.
[13] E.J. Gibbins, J.L. Irwin, A.G. Livingston, J.C. Muir, D.A. Patterson, C. Roengpithya, P.C. Taylor, An improved protocol for the synthesis and nanofiltration of Kim and Park's aminocyclopentadienyl ruthenium chloride racemisation catalyst, Synlett 19 (2005) 2993–2995.
[14] E.J. Gibbins, J.L. Irwin, A.G. Livingston, J.C. Muir, D.A. Patterson, C. Roengpithya, P.C. Taylor, Dynamic kinetic resolution of racemates using membrane-separated catalysts, Abstracts of Papers of the American Chemical Society 229 (2005) U550-U550.
[15] D.A. Patterson, L.Y. Lau, C. Roengpithya, E. Gibbins, A.G. Livingston, Membrane selectivity in the organic solvent nanofiltration of trialkylamine bases, Desalination 218 (2007) 248–256.
[16] N.F. Ghazali, D.A. Patterson, A.G. Livingston, Elucidation of the mechanism of diastereomeric salt formation using organic solvent nanofiltration, Chem. Commun. 40 (8) (2004) 962–963.
[17] A. Livingston, L. Peeva, S. Han, D. Nair, S.S. Luthra, L.S. White, L.M. Freitas dos Santos, Membrane separation in green chemical processing—solvent nanofiltration in liquid phase organic synthesis reactions, Ann. N Y Acad. Sci. 984 (2003) 123–141.
[18] J.G. Wijmans, R.W. Baker, The solution-diffusion model: a review, J. Membr. Sci. 107 (1995) 1–21.

[19] R.W. Baker, Membrane Technology and Applications, second ed., John Wiley & Sons Ltd., Chichester, West Sussex, England, 2004.
[20] P. Vandezande, L.E.M. Gevers, I.F.J. Vankelecom, Solvent resistance nanofiltration: separating on a molecular level, Chem. Soc. Rev. (2008) 365–405.
[21] I.F.J. Vankelecom, K. De Smet, L.E.M. Gevers, A. Livingston, D. Nair, S. Aerts, S. Kuypers, P.A. Jacobs, Physico-chemical interpretation of the SRNF transport mechanism for solvents through dense silicone membranes, J. Membr. Sci. 231 (2004) 99–108.
[22] S.S. Luthra, X.J. Yang, L.M.F. Dos Santos, L.S. White, A.G. Livingston, Homogeneous phase transfer catalyst recovery and re-use using solvent resistant membranes, J. Membr. Sci. 201 (2002) 65–75.
[23] I.A. Boiarkine, E.A.C. Emanuelsson, W. Gao, D.A. Patterson, Preliminary investigation of magnetron sputtered thin films as photocatalysts for advanced oxidation, in: Proceedings of Chemeca 2008, Newcastle, Australia, 28 September–1 October, Engineers Australia, ACT, Australia, 2008.
[24] E.A.C. Emanuelsson-Patterson, A.M. Ali, X. Yan, W. Gao, D.A. Patterson, Investigating the correlation between ZnO thin film surface morphologies and photocatalytic activity in the photooxidation of methylene blue, in: Proceedings of Chemeca 2008, Newcastle, Australia, 28 September–1 October, Engineers Australia, ACT, Australia, 2008.
[25] S. Kazama, M. Sakashita, Gas separation properties and morphology of asymmetric hollow fiber membranes made from cardo polyamide, J. Membr. Sci. 243 (2004) 59–68.